

Learning Self-Supervised Low-Rank Network for Single-Stage Weakly and Semi-Supervised Semantic Segmentation

Junwen Pan* · Pengfei Zhu*[†] · Kaihua Zhang · Bing Cao · Yu Wang ·
Dingwen Zhang · Junwei Han · Qinghua Hu

Received: date / Accepted: date

Abstract Semantic segmentation with limited annotations, such as weakly supervised semantic segmentation (WSSS) and semi-supervised semantic segmentation (SSSS), is a challenging task that has attracted much attention recently. Most leading WSSS methods employ a sophisticated multi-stage training strategy to estimate pseudo-labels as precise as possible, but they suffer from high model complexity. In contrast, there exists another research line that trains a single network with image-level labels in one training cycle. However, such a single-stage strategy often performs poorly because of the compounding effect caused by inaccurate pseudo-label estimation. To address this issue, this paper presents a Self-supervised Low-Rank Network (SLRNet) for single-stage WSSS and SSSS. The SLRNet uses cross-view self-supervision, that is, it simultaneously predicts several complementary attentive LR representations from different views of an image to learn precise pseudo-labels. Specifically, we reformulate the LR representation learning as

a collective matrix factorization problem and optimize it jointly with the network learning in an end-to-end manner. The resulting LR representation deprecates noisy information while capturing stable semantics across different views, making it robust to the input variations, thereby reducing overfitting to self-supervision errors. The SLRNet can provide a unified single-stage framework for various label-efficient semantic segmentation settings: 1) WSSS with image-level labeled data, 2) SSSS with a few pixel-level labeled data, and 3) SSSS with a few pixel-level labeled data and many image-level labeled data. Extensive experiments on the Pascal VOC 2012, COCO, and L2ID datasets demonstrate that our SLRNet outperforms both state-of-the-art WSSS and SSSS methods with a variety of different settings, proving its good generalizability and efficacy.

Keywords Weakly-supervised Learning · Semi-supervised Learning · Semantic Segmentation

Junwen Pan
Tianjin University, Tianjin, China
E-mail: junwenpan@tju.edu.cn

Pengfei Zhu
Tianjin University, Tianjin, China
E-mail: zhupengfei@tju.edu.cn
[†] Corresponding author

* These authors contributed equally.

Kaihua Zhang
Nanjing University of Information Science and Technology,
Nanjing, China
E-mail: zhkhua@gmail.com

Bing Cao, Yu Wang and Qinghua Hu
Tianjin University, Tianjin, China

Dingwen Zhang and Junwei Han
Northwestern Polytechnical University, Xi'an, China

1 Introduction

Semantic segmentation is a fundamental computer vision task that aims to assign a label to each pixel, promoting the development of many downstream tasks, such as scene parsing, autonomous driving, and medical image analysis (Chen et al., 2018; Zhou et al., 2019; Havaei et al., 2017). Recently, deep learning based semantic segmentation models (Long et al., 2015; Chen et al., 2018), trained with large-scale data labeled at pixel level, have achieved impressive progress. However, such supervised approaches require intensive manual annotations that are time-consuming and expensive, which have inspired many investigations about learning with low-cost annotations, such as semi-supervised

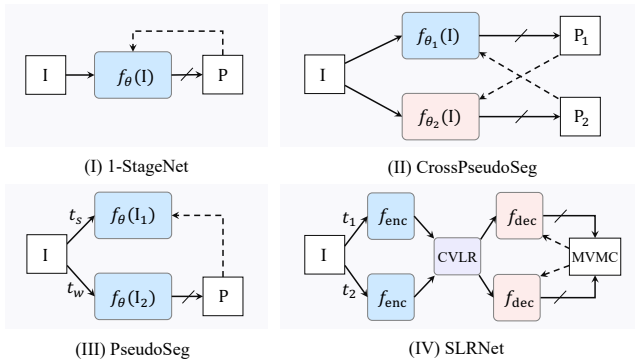


Fig. 1: Overview of pseudo supervision architectures: (I) Single pseudo supervision for WSSS (Araslanov and Roth, 2020), (II) Cross pseudo supervision for SSSS (Chen et al., 2021), (III) PseudoSeg supervision for SSSS (Zou et al., 2021), and (IV) The SLRNet with MVMC and CVLR can mitigate the compounding effect of pseudo supervision error. ‘ \rightarrow ’ means the forward operation, ‘ \dashrightarrow ’ means pseudo supervision, ‘/’ on ‘ \rightarrow ’ means stop-gradient and pseudo-label generation. t denotes the transformation operator, s and w are short for “strong” and “weak” respectively.

semantic segmentation (SSSS) with limited amounts of labeled data, weakly supervised semantic segmentation (WSSS) with bounding boxes (Dai et al., 2015), scribbles (Lin et al., 2016), points (Bearman et al., 2016), and image-level labels (Kolesnikov and Lampert, 2016). Nevertheless, there is a considerable gulf between weakly supervised and semi-supervised approaches.

Most popular image-level WSSS methods (Ahn et al., 2019; Dong et al., 2020; Sun et al., 2020) resort to multiple training and refinement stages to obtain more accurate pseudo-labels while avoiding error accumulation. These methods often start from a weakly supervised localization, such as a class activation map (CAM) (Zhou et al., 2016), which highlights the most discriminative regions in an image. In this approach, diverse enhanced CAM-generating networks (Lee et al., 2019; Wang et al., 2020b; Sun et al., 2020) and CAM-refinement procedures (Ahn and Kwak, 2018; Ahn et al., 2019; Shimoda and Yanai, 2019) have been designed to expand the highlighted area to the entire object or eliminate the wrongly highlighted area. Although these multi-stage methods can produce more accurate pseudo-labels, they suffer from the need of a large number of hyper-parameters and complex training procedures. Single-stage WSSS methods (Zheng et al., 2015; Papandreou et al., 2015) have received less attention because their segmentation is less accurate than that of multi-stage methods. Recently, Araslanov and Roth (2020) proposed a simple single-stage WSSS model that generates pixel-level

pseudo-labels online as self-supervision (Fig. 1 (I)). However, its accuracy is still not comparable with that of multi-stage approaches. In contrast, the simple online pseudo-supervision scheme has made promising progress in SSSS (Fig. 1(II) (Chen et al., 2021) and (III) (Zou et al., 2021)).

We argue that the cause of the inferior performance of the online pseudo supervised WSSS is the compounding effect of errors caused by online inaccurate pseudo supervision. Like multi-stage refinements, online pseudo-label supervision should gradually improve the semantic fidelity and completeness during the training process. However, this also increases the risk that errors are mimicked and accumulated with the gradient flows being backpropagated from the top to the lower layers. Consistency learning is widely used as additional supervision to semi-supervised learning (Ouali et al., 2020; Chen et al., 2021). However, in practice, existing consistency-based methods are not applicable to image-level weakly supervised settings. First, they require pixel-level supervision to avoid the collapsing solution (Chen and He, 2021). Second, the dominance of consistency harms the region expansion for WSSS.

To this end, we propose the **Self-supervised Low-Rank Network** (SLRNet) for single-stage WSSS and SSSS. As illustrated in Fig. 1(IV), the SLRNet simultaneously predicts several segmentation masks for various augmented versions of one image, which are jointly calibrated and refined by a multi-view mask calibration (MVMC) module to generate one pseudo-mask for self-supervision. The pseudo-mask leverages the complementary information from various augmented views, which enforces the cross-view consistency on the predictions. To further regularize the network, the SLRNet introduces the LR inductive bias implemented by a cross-view low-rank (CVLR) module. The CVLR exploits the collective matrix factorization to jointly decompose the learned representations from different views into sub-matrices while recovering a clean LR signal subspace. Through the dictionary shared over different views, a variety of related features from various views can be refined and amplified to eliminate the ambiguities or false predictions. Thereby, the input features of the decoder deprecate noisy information, and this can effectively prevent the network from overfitting to the false pseudo-labels. Additionally, instead of directly randomly initializing the sub-matrices, a latent space regularization is designed to improve the optimization efficiency.

The SLRNet is an efficient and elegant framework that generalizes well to different label-efficient segmentation settings without additional training phases.

For instance, to simultaneously utilize image-level and pixel-level labels, previous SSSS methods (Lee et al., 2019; Wei et al., 2018) have to generate and refine pseudo-labels *offline* using WSSS model, which are bundled with pixel-level labels to train a network in the next stage. Such a multi-stage scheme provides a marginal improvement over dedicated SSSS algorithms (Ouali et al., 2020; Zou et al., 2021) with unlabeled data. In contrast, the SLRNet directly introduces additional pixel-level supervision while combining it with image-level data without extra cost. In other words, the online pseudo-mask generation takes into account both image-level and pixel-level labels in a single training phase and is undoubtedly more accurate. To the best of our knowledge, the SLRNet is the first attempt to bridge these tasks into a unified single-stage scheme, allowing it to maximize exploiting various annotations with a limited budget.

In our experiments, we first validate the performance of SLRNet in an image-level WSSS setting on several datasets, including Pascal VOC 2012 (Everingham et al., 2010), COCO (Lin et al., 2014), and L2ID (Wei et al., 2020). Extensive experiments demonstrate that the cross-view supervision and the CVLR help improve semantic fidelity and completeness of the generated segmentation masks. Notably, the SLRNet also establishes new state-of-the-arts for various label-efficient semantic segmentation tasks, including 1) WSSS with image-level labeled data, 2) SSSS with pixel-level and image-level labeled data and 3) SSSS with pixel-level labeled and unlabeled data. Moreover, the SLRNet achieves the best performance at the WSSS Track of CVPR 2021 Learning from Limited and Imperfect Data (L2ID) Challenge (Wei et al., 2020), outperforming other competitors by large margins of $\sim 9.35\%$ in terms of mIoU.

The main contributions of this work are summarized as follows:

- 1) We propose an effective cross-view self-supervision scheme, incorporating the CVLR module, to alleviate the compounding effect of self-supervision errors for the online pseudo-label training.
- 2) We present a plug-and-play collective matrix factorization method with latent space regularization for multi-view LR representation learning, which can be readily embedded into any Siamese networks for end-to-end training.
- 3) The SLRNet provides a unified framework that can be well generalized to learn a segmentation model from different limited annotations in various WSSS and SSSS settings.
- 4) The SLRNet achieves leading performance compared to a variety of state-of-the-art methods on

Pascal VOC 2012, COCO, and L2ID datasets for both WSSS and SSSS tasks.

2 Related Work

This section reviews a variety of methods related to the proposed SLRNet, including the WSSS, the SSSS, the LR representation, and the self-supervised learning methods.

2.1 Weakly Supervised Semantic Segmentation

In the past years, various variants of WSSS methods have been developed and evolved rapidly, which can be categorized into multi-stage and single-stage classes. Most multi-stage WSSS methods with image-level supervision start from the CAM (Zhou et al., 2016). These methods refine the CAM obtained from a pre-trained CAM-generating (classification) network to generate segmentation pseudo-labels, with the aim of expanding the highlighted area to the entire object or eliminating the false highlighted area. The prevailing method is to consider the semantic completeness and fidelity of the seed region when training the CAM-generating network using, for instance, atrous convolution (Wei et al., 2018), stochastic feature selection (Lee et al., 2019), the idea of erasing (Wei et al., 2017; Hou et al., 2017), cross-image affinity (Sun et al., 2020), and the equivariant for various scaled input images (Wang et al., 2020b). Although the seed obtained from an improved CAM-generating network is better, most of these methods still need extra CAM-refinement procedures, such as random walk (Ahn and Kwak, 2018), region growing (Huang et al., 2018), or an additional network for distillation. Moreover, some of these methods utilize class-agnostic saliency maps to obtain background cues. The multi-stage methods use a series of algorithms to improve the WSSS accuracy by carefully tuning the hyperparameters of each stage, leading to a rapid increase in complexity.

In contrast to the multi-stage methods, the single-stage approaches train WSSS models using only one training cycle (Pinheiro and Collobert, 2015; Papandreou et al., 2015; Zheng et al., 2015), but they cannot perform favorably because of their inferior segmentation accuracy. Recently, (Araslanov and Roth, 2020) proposed a simple yet effective single-stage model, *i.e.*, they train a segmentation network with image-level labels and produce refined masks online as self-supervision. However, this self-trained model is still unable to compete with the latest multi-stage

methods [Ahn et al. \(2019\)](#); [Lee et al. \(2019\)](#); [Wang et al. \(2020b\)](#) in accuracy.

2.2 Semi-Supervised Semantic Segmentation

Generally, in semi-supervised learning, only a small subset of training images are assumed to have annotations, and a large number of unlabeled data are exploited to improve performance. Early SSSS models ([Hung et al., 2018](#); [Souly et al., 2017](#)) based on generative adversarial networks learn a discriminator between the prediction and the ground truth mask or generate additional training data. Recently, consistency based approaches have been extensively explored. These approaches enforce the predictions to be consistent, either using transformed input images ([French et al., 2020](#); [Zou et al., 2021](#)), perturbed feature representations ([Ouali et al., 2020](#)), or different networks ([Chen et al., 2021](#)). PseudoSeg ([Zou et al., 2021](#)) and CrossPseudo ([Chen et al., 2021](#)) realize the idea of consistency by designing pseudo-labels online to encourage the cross-view consistency, *i.e.*, one view generates pseudo-labels for supervising another view, instead of explicitly enforcing the prediction consistency. In this paper, our experiments illustrate that this explicit consistency impairs the expansion of highlighted regions under a weakly supervised setting.

Another WSSS-based line of research involves harnessing low-cost image-level supervision. As described in [Sec. 2.1](#), WSSS approaches generate segmentation pseudo-labels that can then be used to train a segmentation network together with the human-annotated pixel-level labels ([Lee et al., 2019](#); [Wei et al., 2018](#); [Li et al., 2018](#)). In contrast, our SLRNet provides a unified single-stage WSSS and SSSS framework without offline pseudo-label generation or multi-stage training.

2.3 Low-Rank Representation

The LR representation seeks a compact data structure and has been widely applied to subspace clustering ([Liu et al., 2012](#)), dictionary learning ([Ma et al., 2012](#)), matrix decomposition ([Cabral et al., 2013](#)), and deep network approximation ([Tai et al., 2016](#)). Liu et al. proposed a robust subspace clustering model using an LR representation ([Liu et al., 2012](#)); Ma et al. proposed a discriminative LR dictionary learning algorithm for face recognition ([Ma et al., 2012](#)); and Ricardo et al. proposed a unified approach to bilinear factorization and nuclear norm regularization for LR matrix decomposition ([Cabral et al., 2013](#)). Because of the redundancy of convolutional filters, LR regularization is imposed

to speed up convolutional neural networks ([Tai et al., 2016](#)). Recently, [Geng et al. \(2021\)](#) and [Li et al. \(2019\)](#) introduced the LR reconstruction into segmentation as an alternative to the self-attention mechanism. Both of them merely endeavor to denoise variance and capture the invariant representations between related pixels in a single feature map, while ignoring the inconsistency and noise in cross-view feature maps, and thus can bring a rather marginal effect towards alleviating the error accumulation in those settings with limited supervision.

2.4 Self-Supervised Learning

Self-supervised learning aims at designing pretext tasks to learn general feature representations from large-scale unlabeled data without human-annotated labels. Classical pretext tasks include image and video generation ([Pathak et al., 2016](#); [Ledig et al., 2017](#)), spatial or temporal context learning ([Doersch et al., 2015](#); [Lee et al., 2017](#)), and free semantic label-based methods ([Stretcu and Leordeanu, 2015](#)). Recently, contrastive learning has become popular, whose core idea is to attract positive pairs and repulse negative pairs ([Chen et al., 2020](#); [He et al., 2020](#)). Siamese architectures for contrastive learning can model transformation invariance by weight-sharing, *i.e.*, two views of the same sample should produce the consistent outputs ([Chen and He, 2021](#)). The pre-trained features by self-supervised methods are transferred to the downstream tasks for further learning. For downstream tasks requiring dense predictions (*e.g.*, segmentation and detection), there are also a flurry of recent work ([Xie et al., 2021a,b](#); [Wang et al., 2021](#); [O. Pinheiro et al., 2020](#)) exploring pixel-level contrastive learning that model local invariance by considering the correspondence between local representations.

Considering the label-efficient segmentation with limited supervision signal, it is intuitive to introduce self-supervision as additional constraint to narrow the gap between label-efficient and fully-supervised settings. SEAM ([Wang et al., 2020b](#)) exploited a Siamese network to model scale equivariance, while CIAN ([Fan et al., 2020](#)) and MCIS ([Sun et al., 2020](#)) mined the cross-image affinity from image pairs. Here, self-supervision is manifested in distinct dimensions: along with pixel-level prediction consistency over different transformed views, free pseudo ground-truth calibrated by the MVMC can also be regarded as self-supervision. Additionally, the CVLR enforces consistency between cluster assignments produced for different views, which is also related to self-supervised SWaV ([Caron et al., 2020](#)).

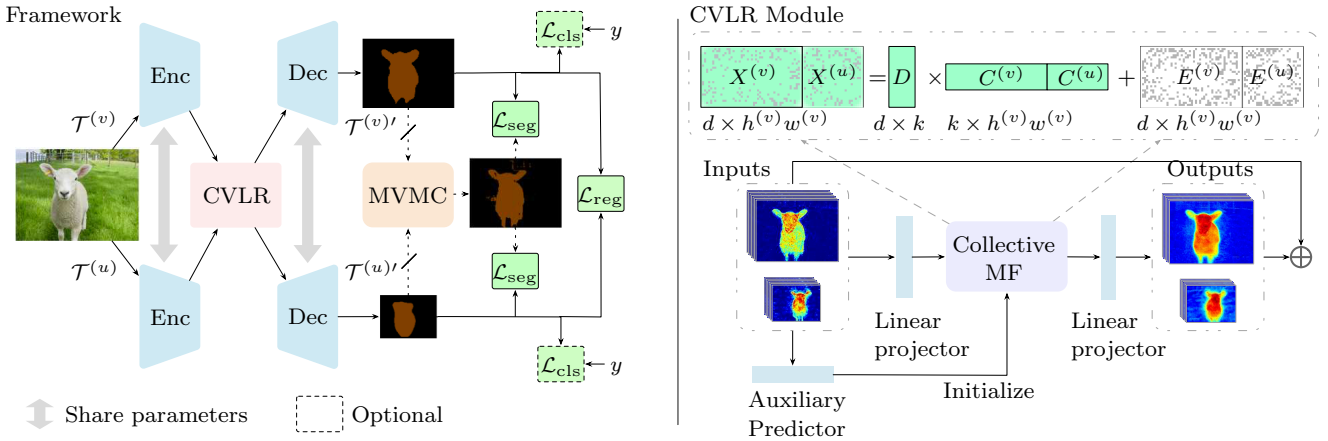


Fig. 2: **Left:** Architecture of the proposed SLRNet. The SLRNet is a multi-branch network with shared parameters, which simultaneously predicts the masks of multiple views (v and u) from one image. The MVMC generates a pseudo segmentation mask as self-supervision (using loss \mathcal{L}_{seg}) by calibrating the false activations in these predicted masks. Meanwhile, the outputs are also constrained by image-level loss \mathcal{L}_{cls} and explicit cross-view regularization \mathcal{L}_{reg} . **Right:** The CVLR module. The CVLR is implemented by the cross-view matrix factorization, which reduces the multi-view features into a shared dictionary (\mathbf{D}) and a set of code matrices (\mathbf{C}^v), where the noises are removed during the reconstruction.

3 Methodology

This section introduces the proposed SLRNet in details. First, we introduce the unified framework of SLRNet for label-efficient semantic segmentation in Sec. 3.1. Then, we introduce how to design the cross-view supervision in Sec. 3.2. Among it, to reduce the compounding effect caused by self-supervision errors, the MVMC method is proposed to provide cross-view pseudo-label supervision. Finally, Sec. 3.3 introduces the CVLR model, among which we introduce the inductive bias of the LR property into the neural network using the collective matrix factorization method to further mitigate the compounding effect of errors. The CVLR module is then integrated into the network for end-to-end training.

3.1 Framework of the SLRNet

Similar to typical fully-supervised semantic segmentation, the SLRNet consists of one network trained in one stage without complicated steps for both WSSS and SSSS tasks in a unified framework. Specifically, the SLRNet expands the established encoder–decoder segmentation network (Chen et al., 2018) into a simple shared-weight Siamese structure (Fig. 2 left). The SLRNet takes m views $\mathbf{I}^{(v)}$ from an image \mathbf{I} augmented by transformations $\mathcal{T}^{(v)}$ as input. For explanation clarity, the superscript v denotes the index of view $v \in \mathcal{V}$ and $|\mathcal{V}|$ denotes the total number of views. The encoder net-

work processes these views and produces feature maps $\mathbf{X}^{(v)} \in \mathbb{R}^{h^{(v)} \times w^{(v)} \times d}$. The CVLR module in Sec. 3.3 jointly factorizes the high-dimensional noisy features $\mathbf{X}^{(v)}$ from different views into sub-matrices and reconstructs the LR features $\tilde{\mathbf{X}}^{(v)}$. Afterwards, the features with the LR property are fed to the decoder to predict the segmentation logits $\hat{\mathbf{M}}^{(v)}$.

From a unified perspective, we consider three typical types of data under established label-efficient settings: pixel-level labeled data $\mathcal{D}_p \in \{(\mathbf{I}_i, \mathbf{M}_i)\}_{i=1}^{|\mathcal{D}_p|}$, image-level (*i.e.* classification) labeled data $\mathcal{D}_c \in \{(\mathbf{I}_i, \mathbf{y}_i)\}_{i=1}^{|\mathcal{D}_c|}$, and unlabeled data $\mathcal{D}_u \in \{\mathbf{I}_i\}_{i=1}^{|\mathcal{D}_u|}$. During training, the samples in \mathcal{D}_p use the manually labeled pixel-wise mask \mathbf{M} , and those in \mathcal{D}_c and \mathcal{D}_u use the estimated pseudo-labels $\tilde{\mathbf{M}}$ produced by the MVMC module described in Sec. 3.2 as ground-truth to construct the following pixel-level cross entropy (CE) loss:

$$\begin{aligned} \mathcal{L}_{seg} = & \sum_{i \in \mathcal{D}_p} \sum_{v \in \mathcal{V}} \mathcal{L}_{CE}(\hat{\mathbf{M}}_i^{(v)}, \mathbf{M}_i) \\ & + \sum_{i \in \mathcal{D}_c \cup \mathcal{D}_u} \sum_{v \in \mathcal{V}} \mathcal{L}_{CE}(\hat{\mathbf{M}}_i^{(v)}, \tilde{\mathbf{M}}_i). \end{aligned} \quad (1)$$

We apply normalized global weighted pooling with focal mask penalty (Araslanov and Roth, 2020) on the mask logits $\mathbf{M}^{(v)}$ to obtain class scores $\hat{\mathbf{y}}^{(v)} = pool(\mathbf{M}^{(v)})$. Besides, we employ the binary cross entropy (BCE) (Paszke et al., 2019) for multi-label one-versus-all classification defined as follows:

$$\mathcal{L}_{cls} = \sum_{i \in \mathcal{D}_c} \sum_{v \in \mathcal{V}} \mathcal{L}_{BCE}(\hat{\mathbf{y}}_i^{(v)}, \mathbf{y}_i). \quad (2)$$

3.2 Cross-view Supervision

The SLRNet employs pixel-level pseudo-labels generated online for self-supervision. How to generate the desired pseudo-mask $\hat{\mathbf{M}}$ is a pivotal question. A naive solution is to simply utilize the decoder output of a trained model after confidence thresholding, as suggested by Zoph et al. (2020); Sohn et al. (2020). However, in a label-efficient segmentation regime, especially in image-level WSSS, the generated hard/soft pseudo-mask is fairly coarse. As the network becomes deeper and deeper, errors are prone to be accumulated as the gradient flows are backpropagated from the top to the lower layers, and thus yield inferior performance (Chen et al., 2018; Araslanov and Roth, 2020). We use two distinct yet efficient insights to generate better pseudo-label masks: First, we use the complementary information through multi-view fusion to eliminate potential errors in the decoder outputs; Second, we utilize explicit and implicit cross-view supervision to regularize the network to produce more consistent outputs.

Multi-view Mask Calibration. Most previous WSSS approaches employ *offline* multi-scale ensemble (*i.e.* test-time augmentation) and complicated post-processing steps (*e.g.* Ahn and Kwak (2018); Ahn et al. (2019); Dong et al. (2020)) to refine the coarse outputs as pseudo-labels. These approaches require multi-stage training that increases model complexity. Here, we present an efficient and effective *online* MVMC scheme for mask calibration. In the early training steps, the network’s output is prone to activate partial regions of interest or too many background regions, whereas we can use the output of different augmented versions to calibrate the false predictions. Specifically, the network simultaneously predicts a set of masks $\{\mathbf{M}^{(v)} \in \mathbb{R}^{h^{(v)} \times h^{(v)} \times d}\}_{v \in \mathcal{V}}$ for various transformed versions of the same image whose spatial pixels are not aligned because of various geometric transformations. First, the output $\hat{\mathbf{M}}^{(v)}$ is transformed respectively by the inverse geometric transformations $\mathcal{T}^{(v)'}$. Note that we assume that $\mathcal{T}^{(v)'}$ is “differentiable”, *e.g.*, we use bilinear interpolation and flipping. Then, the fused masks are processed by the refinement procedure \mathcal{R} . The whole calibration process can be formulated as:

$$\tilde{\mathbf{M}} = \mathcal{R} \left(\text{softmax} \left(\frac{\sum_{v \in \mathcal{V}} \mathcal{T}^{(v)'(\mathbf{M}^{(v)})}}{|\mathcal{V}|} \right) \right). \quad (3)$$

Because a classic refinement algorithm such as dense CRF (Krähenbühl and Koltun, 2011) slows down the training process, we refine the coarse masks with respect to appearance affinities through pixel-adaptive convolution (Su et al., 2019; Araslanov and Roth, 2020).

To generate the one-hot hard pseudo-labels, we retain the pseudo-labels of pixels with confidence higher than a threshold γ , and ignore the pixels with low confidence or those belonging to multiple categories.

Implicit and Explicit Cross-view Supervision. The pseudo-masks produced by the MVMC utilize the complementary information from different views, and hence the pseudo supervised segmentation loss in Eq. 1 implicitly enforces prediction consistency. In contrast to PseudoSeg (Zou et al., 2021) and CPS (Chen et al., 2021), which explicitly realize cross-view supervision, the proposed approach implicitly implements cross-view consistency regularization and exploits the MVMC to filter out false pseudo-labels. Extensively investigations reveal that pure cross-view supervision is prone to cause mode collapse in unsupervised settings (Chen and He, 2021; Chen et al., 2020). In practice, our experiments in Sec. 4.6 also show that the dominance of explicit cross-view supervision can compromise the semantic completeness in WSSS. Therefore, a proper and adjustable cross-view supervision strength is crucial in the settings with limited supervision. Here, we define an explicit consistency loss, which is tuned by a scaling factor λ_{reg} , to compensate for the implicit cross-view consistency:

$$\mathcal{L}_{\text{reg}}^{\text{mask}} = \sum_{i \in \mathcal{D}} \sum_{v, u \in \mathcal{V}, v \neq u} \sum_{c \in \mathbf{y}_i} s \left[\mathcal{T}^{(v)' \left(\hat{\mathbf{M}}_{i,c}^{(v)} \right), \mathcal{T}^{(u)' \left(\hat{\mathbf{M}}_{i,c}^{(u)} \right)} \right], \quad (4)$$

where $s(\cdot, \cdot)$ is a distance measure between two output masks, $\mathcal{D} = \mathcal{D}_p \cup \mathcal{D}_c \cup \mathcal{D}_u$ denotes all samples, and (v, u) denotes the pairs composed of different views. We consider only the mask of category c contained in the classification label \mathbf{y}_i for the i -th example. For unlabeled sample $i \in \mathcal{D}_u$, all categories are involved in the computation.

3.3 Cross-view Low-Rank Module

Although the MVMC can provide more accurate pseudo-label mask and regularization effect, there still exist a lot of clutter and incompleteness in pseudo-masks. To further reduce the compounding effect of self-supervision errors, we introduce an additional inductive bias, *i.e.*, the LR property of the cross-view deep embeddings, and formulate it into an optimization objective in terms of collective matrix factorization. Fig. 2 (right) illustrates the architecture of the CVLR module. Its essence lies in capturing the invariant LR feature representations from differently transformed views to reduce the accumulated errors introduced by distorted and noisy self-supervision.

Algorithm 1: Collective MF

Input: $\mathbf{X} = \{\mathbf{X}^{(v)} \in \mathbb{R}^{d \times h^{(v)} w^{(v)}}\}_{v \in \mathcal{V}}$, $\mathbf{D} \in \mathbb{R}^{d \times k}$,
 $\mathbf{C} = \{\mathbf{C}^{(v)} \in \mathbb{R}^{k \times h^{(v)} w^{(v)}}\}_{v \in \mathcal{V}}$

- 1 **for** $t \leftarrow 1$ **to** T **do**
- 2 $\mathbf{D} \leftarrow \sum_{v \in \mathcal{V}} \mathbf{X}^{(v)} \mathbf{C}^{(v)\top} \mathbf{S}^{-1}$, where
 $\mathbf{S} = \text{diag}(\sum_{v \in \mathcal{V}} \mathbf{C}^{(v)} \mathbf{1}_n)$;
- 3 $\mathbf{C} \leftarrow \{\text{softmax}(\frac{1}{\tau} \mathbf{D}_{\text{norm}}^\top \cdot \mathbf{X}^{(v)}, \text{axis} = 0)\}_{v \in \mathcal{V}}$,
 where $\mathbf{D}_{\text{norm}} = \left[\frac{\mathbf{d}_1}{\|\mathbf{d}_1\|_2}; \dots; \frac{\mathbf{d}_k}{\|\mathbf{d}_k\|_2} \right]$;
- 4 **end**
- 5 $\tilde{\mathbf{X}} \leftarrow \{\tilde{\mathbf{X}}^{(v)} = \mathbf{D}\mathbf{C}^{(v)}\}_{v \in \mathcal{V}}$

Output: $\tilde{\mathbf{X}}$

Matrix Factorization (MF). Before introducing the proposed CVLR module, we first review the key concept of LR MF. The MF reduces a matrix into constituent parts, which disentangles latent structures in high-dimensional complex data. Given n data features of dimension d denoted as $\mathbf{X} = [\mathbf{x}_1; \dots; \mathbf{x}_n] \in \mathbb{R}^{d \times n}$, we assume that there is a low-dimensional subspace hidden in \mathbf{X} . Therefore, \mathbf{X} can be decomposed into a dictionary matrix $\mathbf{D} = [\mathbf{d}_1; \dots; \mathbf{d}_k] \in \mathbb{R}^{d \times k}$ and an associated code matrix $\mathbf{C} = [\mathbf{c}_1; \dots; \mathbf{c}_n] \in \mathbb{R}^{k \times n}$:

$$\mathbf{X} = \tilde{\mathbf{X}} + \mathbf{E} = \mathbf{D}\mathbf{C} + \mathbf{E}, \quad (5)$$

where we denote the reconstructed feature as $\tilde{\mathbf{X}} \in \mathbb{R}^{n \times d}$ and the noise matrix as $\mathbf{E} \in \mathbb{R}^{n \times d}$. \mathbf{E} is discarded in the reconstruction. We assume $k \ll \min(n, d)$, thus $\tilde{\mathbf{X}}$ has the LR property:

$$\text{rank}(\tilde{\mathbf{X}}) \leq \min(\text{rank}(\mathbf{D}), \text{rank}(\mathbf{C})) \leq k \ll \min(d, n). \quad (6)$$

Vector Quantization (VQ). VQ is a classic data compression method, which can be formulated as an optimization objective in terms of MF:

$$\min_{D, C} \|\mathbf{X} - \mathbf{D}\mathbf{C}\|_F \quad \text{s.t. } c_{ij} \in \{0, 1\}, \sum_i c_{ij} = 1, \quad (7)$$

where vector \mathbf{c}_j is a one-hot encoding, which implies a crisp partitioning.

Collective MF. We investigate the idea of collective MF to learn shared latent factors from $|\mathcal{V}|$ matrices of multi-view features. Different views use the same LR representation as part of the approximation, enabling feature sharing and interaction. The objective function of Collective MF can be formalized as:

$$\min_{D, \{C^{(v)}\}} \sum_{v \in \mathcal{V}} \left(\left\| \mathbf{X}^{(v)} - \mathbf{D}\mathbf{C}^{(v)} \right\|_F + r(\mathbf{C}^{(v)}) \right), \quad (8)$$

where r is the regularization term. To minimize the objective function, we utilize the same alternating minimization method as VQ, which is also equivalent to K-means clustering (Gray and Neuhoff, 1998).

We now describe a single iteration on a set of flattened deep feature matrices from various transformed views $\{\mathbf{X}^{(v)} \in \mathbb{R}^{d \times h^{(v)} w^{(v)}}\}_{v \in \mathcal{V}}$. We exploit the weighted mean over varied augmented features to update the shared dictionary matrix \mathbf{D} (Line 2 in Algorithm 1), where the weight $\mathbf{C}^{(v)\top} \mathbf{S}^{-1}$ is calculated over the global codes. Factor matrix $\mathbf{C}^{(v)} \in \mathbb{R}^{k \times h^{(v)} w^{(v)}}$ is computed via the softmax-normalized attention (Vaswani et al., 2017) with temperature coefficient τ instead of the hard maximum, which enables the gradients to be backpropagated. Here we normalize each vector in \mathbf{D} and set $\tau = 1$ by default. As described in Algorithm 1, the CVLR updates the factor matrices \mathbf{D} and $\{\mathbf{C}^{(v)}\}_{v \in \mathcal{V}}$ alternately. After T iterations, the converged \mathbf{D} and $\{\mathbf{C}^{(v)}\}_{v \in \mathcal{V}}$ are used to approximate input features $\{\mathbf{X}^{(v)}\}_{v \in \mathcal{V}}$. As discussed above, the re-estimated matrices $\{\tilde{\mathbf{X}}^{(v)}\}_{v \in \mathcal{V}}$ are endowed with the LR property.

With the above optimization, the features of various transformed views interact with each other iteratively and are compressed into a shared dictionary \mathbf{D} . Then, these condensed semantics are propagated into individual views in the final reconstruction step. From an intuitive perspective, as illustrated in Fig. 2, the re-estimated LR features amplify and refine the related features from complementary views, eliminate ambiguity or false responses, and thus produce more complete and clean activation regions.

Training with Back-Propagation. The above optimization is differentiable with respect to its parameters, which makes it suitable to incorporate with a convolutional neural network for end-to-end training. However, the alternating minimization introduces recurrent neural network-like behavior, and randomly initialized factor matrices require multiple iterations, which will degrade performance due to the vanishing gradient in practice. One possible solution is to stop the gradient flow in the iterations to avoid gradient instability and memorize the previous \mathbf{D} to initialize the current optimization to reduce the number of iterations T (Li et al., 2019). In contrast, the gradient flow is allowed in CVLR and factor $\mathbf{C}^{(v)}$ is initialized with the feature map produced by the network. Given feature map $\mathbf{Z}^{(v)} \in \mathbb{R}^{k \times h^{(v)} w^{(v)}}$, $\text{softmax}(\mathbf{Z}^{(v)}, \text{axis} = 0)$ can be regarded as a good initialization of $\mathbf{C}^{(v)}$. In contrast to random initialization, the optimization swiftly converges within a small number of iterations T .

Latent Space Regularization. For specific scenarios, there are diverse MF variants with various regularizations on \mathbf{D} and \mathbf{C} , such as non-negativity (Lee and Seung, 1999), orthogonality (Ding et al., 2006) and latent space enforcement (Hu et al., 2013). Here, although multi-view features are compressed into a shared dictionary, features with the same semantic meaning may still be assigned to different elements in \mathbf{D} . To this end, we regularize the latent space of code matrix $\mathbf{C}^{(v)}$ to be the pixel-level classification space by fully exploiting the limited supervision. That is, we set the dimension k of the factor matrices to the number of categories provide auxiliary supervision on the initialization of $\mathbf{C}^{(v)}$. In this way, each element in \mathbf{D} is assigned a specific meaning, ensuring cross-view invariance of the reconstructed LR representations. In addition, a cross-view regularization loss on the code matrix \mathbf{C} is designed to encourage the cross-view consistency as follows:

$$\mathcal{L}_{\text{reg}}^{\text{fact}} = \sum_{v,u \in \mathcal{V}, i \neq j} s(\mathcal{T}^{(v)'}(\mathbf{C}^{(v)}), \mathcal{T}^{(u)'}(\mathbf{C}^{(u)})), \quad (9)$$

where $s(\cdot, \cdot)$ is a similarity measure, $\mathcal{T}^{(v)'}$ and $\mathcal{T}^{(u)'}$ are inverse geometric transformations.

Detailed CVLR Module Design. Fig. 2 presents the architecture of CVLR, which collaborates with the networks via two linear projectors and a skip connection. Specifically, a learnable linear transformation maps the inputs to a feature space, and another one maps the approximation $\tilde{\mathbf{X}}$ to the input space. To produce the feature $\mathbf{Z}^{(v)}$ as the initialization of $\mathbf{C}^{(v)}$, the auxiliary prediction head is composed of two convolutional layers supervised by the loss functions defined in Eq. 1 and Eq. 2.

4 Experiments

Implementation Details. In our experiments, WideResNet-38 (Wu et al., 2019) pre-trained on ImageNet (Deng et al., 2009) and atrous spatial pyramid pooling (ASPP) (Chen et al., 2018) form our encoder. The decoder consists of three convolutional layers and a stochastic gate (Araslanov and Roth, 2020), which mixes shallow and deep features. We trained our model for 20 epochs with a stochastic gradient descent optimizer using a weight decay of 5×10^{-4} . The learning rate was set to 5×10^{-3} for randomly initialized parameters and 5×10^{-4} for pre-trained parameters. We use L1 distance as the similarity measure $s(\cdot, \cdot)$ in Eq. 4 and Eq. 9. The final loss function can be expressed as

Method	CRF	train(%)	val(%)
CAM (Ahn and Kwak, 2018)		48.0	46.8
SCE (Chang et al., 2020)		50.9	49.6
SEAM (Wang et al., 2020b)	✓	56.8	–
CAM+RW (Ahn and Kwak, 2018)	✓	59.7	–
SCE+RW (Chang et al., 2020)		63.4	61.2
1-Stage (Araslanov and Roth, 2020)		64.7	63.4
1-Stage (Araslanov and Roth, 2020)	✓	66.9	65.3
Ours		67.1	66.2
Ours+CRF	✓	70.3	69.3

Table 1: Pseudo-mask quality on the Pascal VOC train and val sets. Here we use image-level labels to filter out false positive errors.

$\mathcal{L} = \lambda_{\text{seg}}\mathcal{L}_{\text{seg}} + \lambda_{\text{cls}}\mathcal{L}_{\text{cls}} + \lambda_{\text{reg}}\mathcal{L}_{\text{reg}}^{\text{mask}} + \lambda_{\text{reg}}\mathcal{L}_{\text{reg}}^{\text{fact}}$. In the first five epochs, the factors of the loss functions were set to $\lambda_{\text{seg}} = 0$, $\lambda_{\text{cls}} = 1$, and $\lambda_{\text{reg}} = 4$. After that, they were set to the default values $\lambda_{\text{seg}} = 1$, $\lambda_{\text{cls}} = 1$ and $\lambda_{\text{reg}} = 4$.

Evaluation Metric. We report the results in terms of the mean of the class-wise intersection over union (mIoU) for all datasets.

4.1 Experiment I: Learning WSSS from Pascal VOC Dataset

Experimental Setup. To evaluate the effectiveness of our SLRNet for WSSS, we conduct experiments on the Pascal VOC 2012 dataset (Everingham et al., 2010), which is a widely-used WSSS benchmark. Following the previous standard practice, we take additional annotations from (Hariharan et al., 2011) to build the augmented training set. In total, 10,582 images are used for training, and 1,449 images are kept for validation. Note that, only image-level annotations are available during weakly-supervised training.

Pseudo-mask Quality. Most of the advanced methods refine the pseudo-masks and distill them into a fully-supervised segmentation network at the last stage. Although the SLRNet does not need intermediate pseudo-masks for further training, Tab. 1 compares our pseudo-mask quality with previous state-of-the-arts. We use image-level ground-truth to filter out false-positive errors following prior practice (*for this experiment only*). Our method achieves superior performance against improved CAM-generating methods (Wang et al., 2020b; Chang et al., 2020), multi-stage CAM-refinement methods (Ahn and Kwak, 2018), and single-stage methods (Araslanov and Roth, 2020).

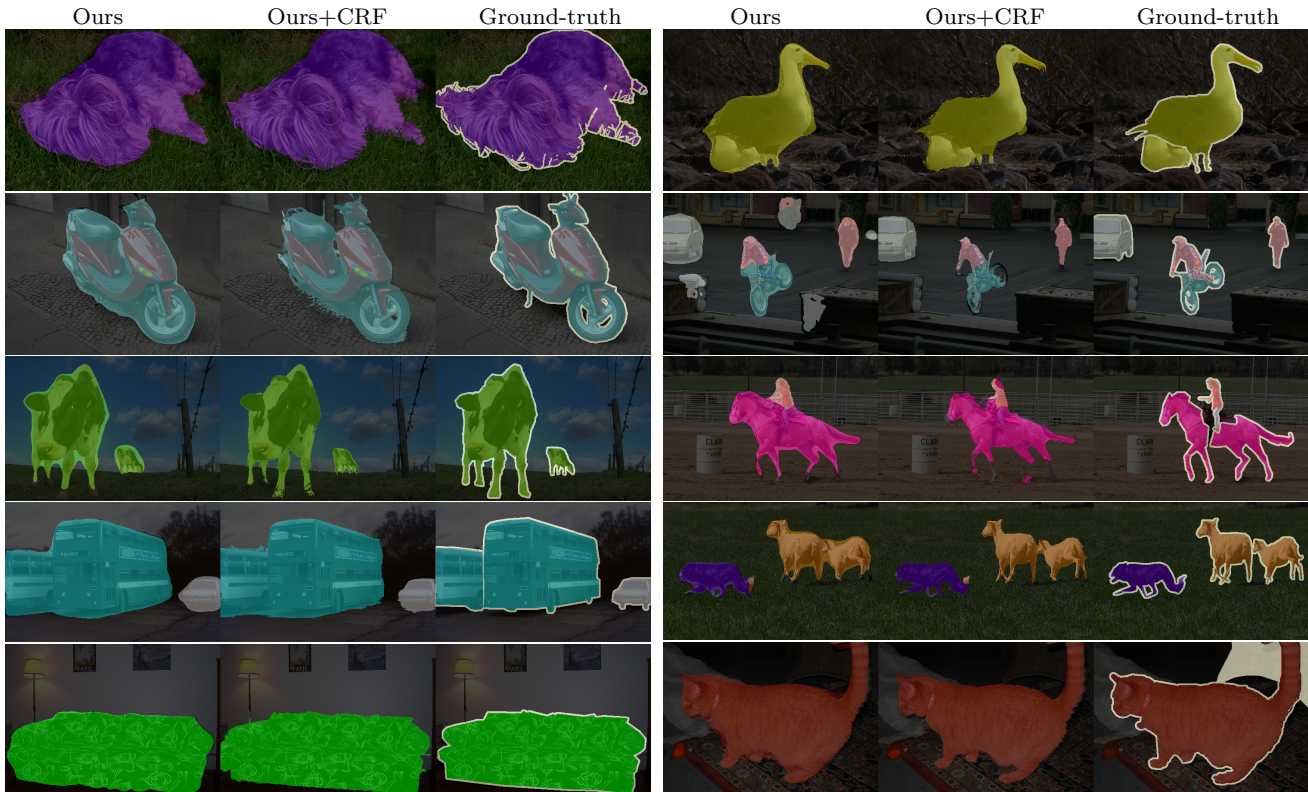


Fig. 3: Qualitative results on Pascal VOC 2012 *val* set. **left**: simple cases. **right**: cases with clutter or incompleteness. The SLRNet produces high-quality segmentation results for challenging scenes with varying object sizes and semantic contents.

Experimental Results. Tab. 2 compares the SLRNet with a variety of leading single- and multi-stage WSSS methods. Among them, the single-stage SLRNet achieves the best performance on both val (67.2%) and test (67.6%) sets. Compared with MCIS (Sun et al., 2020), the current best-performing multi-stage model with saliency maps, our SLRNet obtains an improvement of 1.0% on the val set. Compared with SEAM+CONTA (Dong et al., 2020), that is the current best-performing multi-stage models with WideResNet38 backbone, our SLRNet achieves an mIoU improvement of 1.1%. Note that the compared multi-stage methods without saliency detection are trained in at least *three* stages, which improve performance at the cost of a considerable increase in model complexity. Essentially, CONTA (Dong et al., 2020) is a refinement approach that employs additional networks to revise the masks produced by AffinityNet. SEAM (Wang et al., 2020b) and SCE (Chang et al., 2020) are improved CAM-generating networks which produce the CAMs as AffinityNet’s input. Multi-stage methods improve performance at the cost of a considerable increase in model complexity. Our SLRNet significantly outperforms previous single-stage models

with the help of simple cross-view supervision and the lightweight CVLR. Besides, although it is trivial to train an additional network for distillation, we still provide a simple distilled result for reference.

Qualitative Analysis. Fig. 3 shows some typical qualitative results produced by our SLRNet. Although only trained with image-level supervision, the SLRNet successfully produces high-quality segmentation results for objects of various sizes in various scenarios. In the right side of Fig. 3, we also provide some typical failure cases with clutter or incompleteness, such as interweaving objects and misleading appearance cues.

4.2 Experiment II: Learning WSSS from COCO Dataset

Experimental Setup. COCO (Lin et al., 2014) contains 80 classes, 80k, and 40k images for training and validation. Although pixel-level labels are provided in the COCO dataset, we only used image-level class labels in the training process. Note that *we only sample 50% (40k) of the training images for training to reduce computational costs.*

Method	Backbone	Sup.	val(%)	test(%)
<i>Multi stage (+saliency)</i>				
SEC (Kolesnikov and Lampert, 2016)	VGG16	\mathcal{I}, \mathcal{S}	50.7	51.7
MDC (Wei et al., 2018)	VGG16	\mathcal{I}, \mathcal{S}	60.4	60.8
DSRG (Huang et al., 2018)	ResNet101	\mathcal{I}, \mathcal{S}	61.4	63.2
FickleNet (Lee et al., 2019)	ResNet101	\mathcal{I}, \mathcal{S}	64.9	65.3
CIAN (Fan et al., 2020)	ResNet101	\mathcal{I}, \mathcal{S}	64.3	65.3
MCIS (Sun et al., 2020)	ResNet101	\mathcal{I}, \mathcal{S}	66.2	66.9
<i>Multi stage</i>				
AffinityNet (Ahn and Kwak, 2018)	ResNet38	\mathcal{I}	61.7	63.7
IRN (Ahn et al., 2019)	ResNet50	\mathcal{I}	63.5	64.8
IAL (Wang et al., 2020a)	ResNet38	\mathcal{I}	64.3	65.4
SSDD (Shimoda and Yanai, 2019)	ResNet38	\mathcal{I}	64.9	65.5
SEAM (Wang et al., 2020b)	ResNet38	\mathcal{I}	64.5	65.7
SCE (Chang et al., 2020)	ResNet101	\mathcal{I}	66.1	65.9
CONTA (Dong et al., 2020)	ResNet38	\mathcal{I}	66.1	66.7
<i>Single stage</i>				
EM-Adapt (Papandreou et al., 2015)	VGG16	\mathcal{I}	38.2	39.6
MIL-LSE (Pinheiro and Collobert, 2015)	Overfeat	\mathcal{I}	42.0	40.6
CRF-RNN (Zheng et al., 2015)	VGG16	\mathcal{I}	52.8	53.7
1-Stage (Araslanov and Roth, 2020)	ResNet38	\mathcal{I}	62.7	64.3
SLRNet (ours)	ResNet38	\mathcal{I}	67.2	67.6
SLRNet distilled* (ours)	ResNet38	\mathcal{I}	69.3	69.4

Table 2: Results for WSSS on the Pascal VOC validation and test sets. Cues used for training are given in the ‘‘Sup.’’ column, including image-level labels (\mathcal{I}) and saliency detection (\mathcal{S}). * indicates our *multi-stage* extension: we simply train a DeeplabV3+ network with pseudo-labels generated by SLRNet.

Method	Backbone	mIoU(%)
BFBP (Saleh et al., 2016)	VGG16	20.4
SEC (Kolesnikov and Lampert, 2016)	VGG16	22.4
IAL (Wang et al., 2020a)	ResNet38	27.7
SEAM* (Wang et al., 2020b)	ResNet38	31.9
IRNet* (Ahn et al., 2019)	ResNet50	32.6
SEAM+CONTA (Dong et al., 2020)	ResNet38	32.8
IRNet+CONTA (Dong et al., 2020)	ResNet50	33.4
SLRNet (ours)	ResNet38	35.0

Table 3: Results for WSSS on COCO validation set. * denotes results provided by Dong et al. (2020).

Experimental Results. Tab. 3 compares our approach and current top-leading WSSS methods with image-level supervision on the COCO dataset. We can observe that our method achieves mIoU score of 35.0% on the val set, outperforming all the competitors. When compared with IRNet+CONTA (Dong et al., 2020), the current best-performing method, our approach obtains the improvement of 1.6% with 50% training samples and simple single-stage training. Our SLRNet demonstrates a powerful efficiency and efficacy advan-

Year	Team	Saliency	val(%)	test(%)
LID ₁₉	LEAP_DEXIN	✓	20.67	19.55
	MVN	✓	40.99	40.0
LID ₂₀	UCU&SoftServe		39.65	37.34
	VL-task1		40.08	37.73
	CVL		46.20	45.18
L2ID ₂₁	LEAP Group		40.94	39.03
	NJUST-JDExplore		42.18	39.68
	jszx101		50.90	49.06
	SLRNet (ours)		52.30	49.03

Table 4: Experimental results for WSSS on L2ID validation and test set.

tage when training on large-scale datasets. In contrast, most recent approaches, including SEAM (Wang et al., 2020b), IRNet (Ahn et al., 2019) and CONTA (Dong et al., 2020), require training in *three* or *four* stages and search a large number of hyperparameters for each stage. Moreover, the intermediate results of each stage must be stored on the hard disk which means a huge amount of space and time consumption for large-scale datasets, severely reducing the practicability of WSSS.

4.3 Experiment III: Performance on the WSSS Track of the L2ID Challenge

Experimental Setup. The L2ID challenge dataset (Wei et al., 2020) is built upon the object detection track of ImageNet Large Scale Visual Recognition Competition (ILSVRC) (Deng et al., 2009), which contains 349,319 images with image-level labels from 200 categories. The evaluation is performed on the validation and test sets, which include 4,690 and 10,000 images, respectively. We obtain the pseudo-labels using our single-stage model with mIoU=52.5% on the validation set. Following the previous practice, we train a standalone Deeplabv3+ (Chen et al., 2018) network using pseudo-labels generated by our SLRNet.

Experimental Results. Tab. 4 lists the final results with the mIoU criterion for WSSS track of L2ID challenge, where the top performing methods are included. Our model significantly outperforms the winner of LID 2019, which utilizes saliency maps. In contrast to the champion of LID 2020, the SLRNet is trained in only one cycle to generate pseudo-labels, while the winner integrates the equivariant attention (Wang et al., 2020b) and the co-attention (Sun et al., 2020) to train the classification network, and use the online attention accumulation (Jiang et al., 2019) to generate object localization maps. Besides, it trains the AffinityNet to refine

Method	Backbone	Sup.	val(%)	test(%)
GAIN (Li et al., 2018)	VGG16	$\mathcal{I}, \mathcal{P}, \mathcal{S}$	60.5	62.1
DSRG (Huang et al., 2018)	VGG16	$\mathcal{I}, \mathcal{P}, \mathcal{S}$	64.3	–
MDC (Wei et al., 2018)	VGG16	$\mathcal{I}, \mathcal{P}, \mathcal{S}$	65.7	67.6
FickleNet (Lee et al., 2019)	VGG16	$\mathcal{I}, \mathcal{P}, \mathcal{S}$	65.8	–
GANSeg (Souly et al., 2017)	VGG16	\mathcal{I}, \mathcal{P}	65.8	–
CCT (Ouali et al., 2020)	ResNet50	\mathcal{I}, \mathcal{P}	73.2	–
PseudoSeg (Zou et al., 2021)	ResNet50	\mathcal{I}, \mathcal{P}	73.8	–
SLRNet (ours)	ResNet38	\mathcal{I}, \mathcal{P}	75.1	75.5

Table 5: Experimental results for semi-supervised semantic segmentation on Pascal VOC validation and test set with $9k$ image-level labeled data (\mathcal{I}) and $1.4k$ pixel-level labeled data (\mathcal{P}). We also indicate additional saliency supervision (\mathcal{S}).

the pseudo-labels, and leverages the CRF to refine the final segmentation results. Our model achieves 52.3% mIoU on the validation set and 49.03% mIoU on the test set, respectively, setting a new state-of-the-art on the L2ID challenge through a simple framework.

4.4 Experiment IV: SSSS with Image-level Labeled Dataset and Pixel-level Labeled Dataset

Experimental Setup. To evaluate the proposed method in the semi-supervised setting, we conduct experiments on the Pascal VOC 2012 dataset (Everingham et al., 2010), which is a standard benchmark of SSSS. Following the prior practice, we took 1,449 images with pixel-level labels from the VOC training set and an additional 9,133 images with image-level labels from SBD (Hariharan et al., 2011) to construct the augmented training set. Note that the finely labeled and weakly labeled data are mixed and fed to the network in one training cycle. Intuitively, the finely labeled samples deserve larger weights. We oversample the finely-labeled data by $5\times$ and multiply their loss by a scaling factor of 2. We do not use any additional post-processing methods during testing.

Experimental Results. Tab. 5 lists the comparison results of that our SLRNet to a variety of state-of-the-art methods on the Pascal VOC dataset, where our SLRNet is trained on only 13.8% of images with pixel-level annotations. It achieves an mIoU of 75.1%, which significantly surpasses the WSSS-based methods (Huang et al., 2018; Wei et al., 2018; Lee et al., 2019), GAN-based methods (Souly et al., 2017), and consistency-based methods (Ouali et al., 2020; Zou et al., 2021).

4.5 Experiment V: SSSS with Pixel-level Labeled Dataset and Unlabeled Dataset

Method	Backbone	mIoU (%)
GANSeg (Souly et al., 2017)	VGG16	64.1
AdvSemSeg (Hung et al., 2018)	ResNet101	68.4
CCT (Ouali et al., 2020)	ResNet50	69.4
PseudoSeg (Zou et al., 2021)	ResNet101	72.3
SLRNet (ours)	ResNet38	72.4
	ResNet101	72.9

Table 6: Experimental results for semi-supervised semantic segmentation on the Pascal VOC validation set with $1.4k$ pixel-level labeled data (\mathcal{P}) and $9k$ unlabeled data.

Experimental Setup. We also conduct experiments on the Pascal VOC 2012 dataset (Everingham et al., 2010) using 1,449 pixel-level labeled images and an additional 9,133 unlabeled images.

Experimental Results. Tab. 6 compares the performance of our SLRNet with previous state-of-the-art SSSS methods. It is worth pointing out that we exactly use the same network and hyperparameters as in the image-level WSSS setting. Notwithstanding, the SLRNet still outperforms all the other dedicated SSSS models, illustrating the good versatility and generality of our approach.

4.6 Ablation Study

We conduct ablation experiments on the Pascal VOC dataset for WSSS settings. To demonstrate the improvement source of our SLRNet, we use *mean false discovery rate* (mFDR) and *mean false negative rate* (mFNR) to indicate the semantic fidelity and completeness respectively, which are defined as

$$mFDR = \frac{1}{C} \sum_{c=1}^C \frac{FP_c}{TP_c + FP_c}, \quad (10)$$

and

$$mFNR = \frac{1}{C} \sum_{c=1}^C \frac{FN_c}{TP_c + FN_c}, \quad (11)$$

where TP_c , FP_c , and FN_c denote the number of true positive, false positive and false negative predictions of class c respectively.

#views	scales	color	flip	mIoU(%)
1	(1.0)	✓	✓	60.88
2	(0.5, 1.0)	✓	✓	64.07
	(1.0, 1.0)	✓	✓	61.53
	(0.5, 1.0)	✓		63.89
	(0.5, 1.0)		✓	63.99
3	(0.5, 1.0, 1.5)			63.90

Table 7: Evaluation on different compositions of data augmentation applied on multiple branches. Here, ✓ means that multiple views use the different random transformations (e.g. for color distortion, randomly different distortion strength for different views). No CRF or any other post-processing is used.

Data Augmentation. To understand the effect of individual data augmentation for our SLRNet, we consider several geometric and appearance augmentations in (Chen et al., 2020). Furthermore, we pay more attention to the *invertible* and *differentiable* geometric transformations, such as resizing and flipping. First, the images are randomly cropped to 321×321 . Then, we apply target transformations to different branches. We study the compositions of three kinds of transformations: re-scaling with fixed rates, random horizontal flip and random color distortion (e.g. brightness, contrast, saturation, and hue). Stronger color distortion cannot improve even hurts performance under supervised settings (Chen et al., 2020; Lee et al., 2021). Therefore, we set the maximum strength of color distortion to 0.3 for brightness, contrast, and saturation, and 0.1 for hue component.

Tab. 7 lists evaluation results on the the Pascal VOC val set under different compositions of transformations. We observe that *combination of three different augmentations produces the best performance* (64.07%). When composing more augmentations, cross-view supervision is expected to become much stronger. We also note that *re-scaling contributes a significantly greater improvement than other augmentations*. There is a significant mIoU drop (2.54%) without re-scaling. In contrast, using the same color distortion and flipping for different views leads to a slight mIoU drop (0.08%). The combination of different color distortion and flipping only achieves a minor improvement (0.65%) compared with single-view baseline. Furthermore, it is worth pointing out that although adding more views has higher complexity, this cannot improve the performance. This indicates that the crucial improvement sources are our cross-view design and the LR reconstruction, which require simple augmentations to provide perturbations.

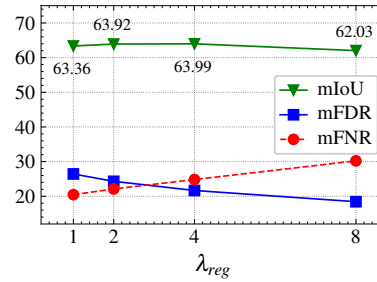


Fig. 4: Ablation study on cross-view supervision. **Left plot:** segmentation performance with varied explicit cross-view supervision strength (λ_{reg}). **Right table:** comparison with other cross-view supervision, including Kullback–Leibler divergence (KL Div.) and cross pseudo supervision (CPS) (Chen et al., 2021).

Cross-view Supervision. Cross-view supervision aims to mitigate the compounding effect of self-supervision errors by introducing additional regularization. We adjust the loss coefficient λ_{reg} that explicitly controls the strength of cross-view supervision. As shown in Fig. 4, we observe that *cross-view supervision mainly improves the segmentation quality by reducing mFDR, i.e., preventing the accumulation of false positives in self-supervision to improve the semantic fidelity*. This improvement is maximized with $\lambda_{reg} = 4$ in our experiments. (For clarification, the scale of \mathcal{L}_{reg} is much smaller than \mathcal{L}_{seg} .) It is worth pointing out that *higher strength of cross-view supervision increases mFNR, i.e., hurts semantic completeness*. Collapsing solutions, where the predictions are all “background”, will occur when explicit cross-view supervision dominates (Chen and He, 2021; Caron et al., 2020). Therefore in the task with limited supervision, choosing appropriate cross-view strength is the crux of performance improvement.

To further validate efficacy of the proposed implicit cross-view supervision, we also compare the MVMC with other cross-view supervision mechanisms. As shown in Fig. 4 (right), we substitute the cross pseudo supervision (Chen et al., 2021) or Kullback–Leibler divergence for MVMC, achieving much worse results. Generally, these explicit consistency methods are applied to SSSS that require pixel-level supervision to avoid collapsing solutions (Chen and He, 2021).

The CVLR Module. To study the effectiveness of each part in the CVLR, we conduct thorough ablation experiments on it. Firstly, as listed in Tab. 8, substituting the shared dictionary matrix with separate ones causes the most severe decay in performance, attesting the significance of the cross-view LR mechanism.

Method	#Iter.	Grad.	mIoU(%)
CVLR	1	yes	63.99
- Separate dictionary \mathbf{D}	1	yes	61.24
- w/o latent space reg.	3	yes	62.83
- w/o CVLR	-	-	61.11
EMAU (Li et al., 2019)	3	no	61.76
Ham. (Geng et al., 2021)	6	1 step	59.75

Table 8: Ablation on shared dictionary \mathbf{D} and latent space regularization. We also provide comparisons between CVLR and other LR modules in terms of iterations (#Iter.) and back-propagation gradients (Grad.).

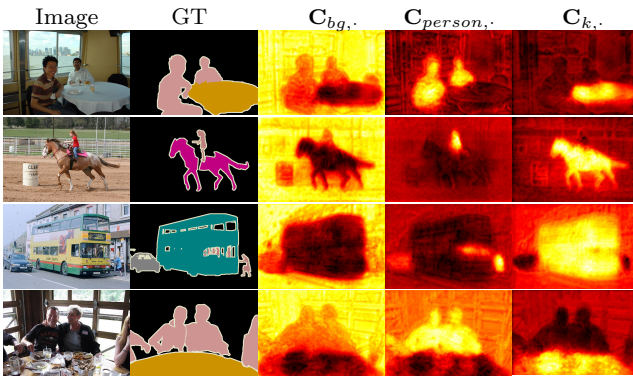


Fig. 5: Visualization of code $\mathbf{C}_{k.}$ for specific item in dictionary \mathbf{D} .

Second, the latent space regularization also contributes considerable performance improvement, as it further enforces the semantic stability and consistency of the elements in the shared dictionary and reduces optimization steps. Furthermore, Tab. 8 compares the CVLR with the EMAU (Li et al., 2019) and the Hamburger (Geng et al., 2021) modules that learn single-view LR representations with specific designs, demonstrating advantages of the proposed CVLR.

To understand and verify the behavior of CVLR, as in Fig. 2 (right), we visualize the feature map before and after the module. The CVLR emphasizes and refines the relevant features from complementary views through reducing ambiguous activation and completing regions. Meanwhile, the proposed latent space regularization allows a close look at the collective matrix factorization, making the factor matrices well interpretable. Fig. 5 visualizes the optimal factor matrix \mathbf{C} (single view is selected) that represents the corresponding probabilities of all pixels to the selected k -th element in the dictionary. The code matrix of specific categories completely highlights the corresponding semantic regions and finely delineates the boundaries.

Another experiment is conducted to explore the impact of hyper-parameters in the CVLR module,

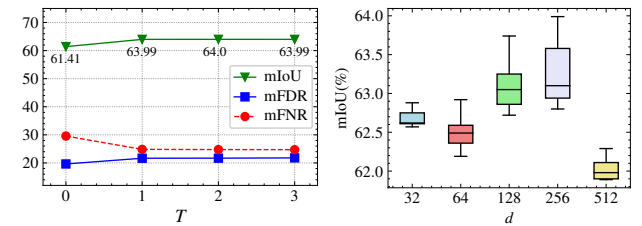


Fig. 6: Ablation on the iteration number T of CVLR and dimension d of the dictionary matrix.

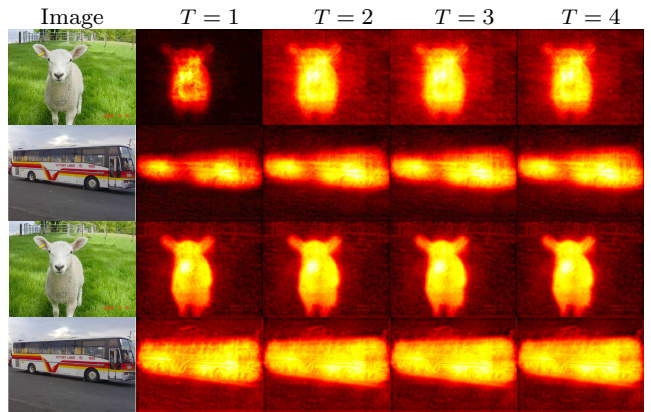


Fig. 7: Visualization of factor $\mathbf{C}_{k.}$ with different iteration number T . The first two rows are from the early training step (randomly selected, epoch=7) and the last two rows are from the last training step (epoch=20).

including optimization step T and latent space dimension d . As shown in Fig. 6 (left), we observe that *the iteration steps improve the segmentation performance mainly by reducing mFNR, i.e., improving the semantic completeness*. We also find that single-step optimization is enough and more iterations cannot improve performance. To empirically analyze this observation, Fig. 7 visualizes the factor matrix $\mathbf{C}_{k.}$ with different number of iterations at different training step. More iterations yield evident effects in the early epochs, while becoming insignificant as the network is converged. Inspired by SimSiam (Chen and He, 2021), we conjecture that the multi-step alternation (inner loop) is optional because the SGD steps provide much more outer loops and the optimization trajectory of the collective MF is memorized by the network parameters. Furthermore, as illustrated in Fig. 6 (right), either too small or too large latent space dimension will negatively impact the segmentation performance and $d = 256$ is the optimal choice in our experiments.

5 Conclusion

This paper has presented a simple yet effective SLRNet for single-stage WSSS and SSSS under online pseudo-label supervision. To overcome the compounding effect of self-supervision errors, we have developed a Siamese network based architecture that makes full use of cross-view supervision and the LR property of the features. Specifically, we have designed the MVMC that aids with explicit cross-view consistency to provide a flexible cross-view supervision solution. Then, we have built a lightweight CVLR module that can be readily integrated into the network for end-to-end training. The CVLR learns an interpretable global cross-view LR representation, which complements cross-view supervision to improve semantic completeness while ensuring semantic fidelity. Despite its simplicity, extensive evaluations have demonstrated that the proposed SLRNet has achieved favorable performance superior to that of both leading single- and multi-stage WSSS and SSSS methods in terms of complexity and accuracy. Our future work is to extend the proposed single-stage model to other label-efficient tasks without the need of considerable training cycles and post-processing techniques.

Acknowledgements This work was partially supported by the National Key Research and Development Program of China under Grant 2019YFB2101904, the National Natural Science Foundation of China under Grants 61732011, 61876127, 61876088 and 61925602.

References

- Ahn J, Kwak S (2018) Learning pixel-level semantic affinity with image-level supervision for weakly supervised semantic segmentation. In: CVPR, pp 4981–4990
- Ahn J, Cho S, Kwak S (2019) Weakly supervised learning of instance segmentation with inter-pixel relations. In: CVPR, pp 2209–2218
- Araslanov N, Roth S (2020) Single-stage semantic segmentation from image labels. In: CVPR, pp 4252–4261
- Bearman A, Russakovsky O, Ferrari V, Fei-Fei L (2016) What’s the point: Semantic segmentation with point supervision. In: ECCV, pp 549–565
- Cabral R, De la Torre F, Costeira JP, Bernardino A (2013) Unifying nuclear norm and bilinear factorization approaches for low-rank matrix decomposition. In: ICCV, pp 2488–2495
- Caron M, Misra I, Mairal J, Goyal P, Bojanowski P, Joulin A (2020) Unsupervised learning of visual features by contrasting cluster assignments. In: NeurIPS
- Chang Y, Wang Q, Hung W, Piramuthu R, Tsai Y, Yang M (2020) Weakly-supervised semantic segmentation via sub-category exploration. In: CVPR, pp 8988–8997
- Chen LC, Zhu Y, Papandreou G, Schroff F, Adam H (2018) Encoder-decoder with atrous separable convolution for semantic image segmentation. In: ECCV, pp 833–851
- Chen T, Kornblith S, Norouzi M, Hinton GE (2020) A simple framework for contrastive learning of visual representations. In: ICML, pp 1597–1607
- Chen X, He K (2021) Exploring simple siamese representation learning. In: CVPR, pp 15750–15758
- Chen X, Yuan Y, Zeng G, Wang J (2021) Semi-supervised semantic segmentation with cross pseudo supervision. In: CVPR, p 0
- Dai J, He K, Sun J (2015) BoxSup: Exploiting bounding boxes to supervise convolutional networks for semantic segmentation. In: CVPR, pp 1635–1643
- Deng J, Dong W, Socher R, Li L, Li K, Li F (2009) Imagenet: A large-scale hierarchical image database. In: CVPR, IEEE Computer Society, pp 248–255
- Ding C, Li T, Peng W, Park H (2006) Orthogonal nonnegative matrix t-factorizations for clustering. In: Proceedings of the 12th ACM SIGKDD International Conference on Knowledge Discovery and Data Mining, p 126–135
- Doersch C, Gupta A, Efros AA (2015) Unsupervised visual representation learning by context prediction. In: ICCV, pp 1422–1430
- Dong Z, Hanwang Z, Jinhui T, Xiansheng H, Qianru S (2020) Causal intervention for weakly supervised semantic segmentation. In: NeurIPS
- Everingham M, Gool LJV, Williams CKI, Winn JM, Zisserman A (2010) The Pascal Visual Object Classes (VOC) Challenge. IJCV 88(2):303–338
- Fan J, Zhang Z, Tan T, Song C, Xiao J (2020) CIAN: cross-image affinity net for weakly supervised semantic segmentation. In: AAAI, pp 10762–10769
- French G, Laine S, Aila T, Mackiewicz M, Finlayson GD (2020) Semi-supervised semantic segmentation needs strong, varied perturbations. In: BMVC
- Geng Z, Guo MH, Chen H, Li X, Wei K, Lin Z (2021) Is attention better than matrix decomposition? In: ICLR
- Gray R, Neuhoff D (1998) Quantization. IEEE Transactions on Information Theory 44(6):2325–2383
- Hariharan B, Arbelaez P, Bourdev LD, Maji S, Malik J (2011) Semantic contours from inverse detectors. In: ICCV, pp 991–998
- Havaei M, Davy A, Warde-Farley D, Biard A, Courville AC, Bengio Y, Pal C, Jodoin P, Larochelle H (2017) Brain tumor segmentation with deep neural net-

- works. *Medical Image Anal* 35:18–31
- He K, Fan H, Wu Y, Xie S, Girshick RB (2020) Momentum contrast for unsupervised visual representation learning. In: *CVPR*, pp 9726–9735
- Hou Q, Jiang P, Wei Y, Cheng M (2017) Self-erasing network for integral object attention. In: *NeurIPS*, pp 547–557
- Hu X, Tang J, Gao H, Liu H (2013) Unsupervised sentiment analysis with emotional signals. In: *22nd International World Wide Web Conference, WWW '13*, Rio de Janeiro, Brazil, May 13-17, 2013, pp 607–618
- Huang Z, Wang X, Wang J, Liu W, Wang J (2018) Weakly-supervised semantic segmentation network with deep seeded region growing. In: *CVPR*, pp 7014–7023
- Hung W, Tsai Y, Liou Y, Lin Y, Yang M (2018) Adversarial learning for semi-supervised semantic segmentation. In: *BMVC*, p 65
- Jiang P, Hou Q, Cao Y, Cheng M, Wei Y, Xiong H (2019) Integral object mining via online attention accumulation. In: *ICCV, IEEE*, pp 2070–2079
- Kolesnikov A, Lampert CH (2016) Seed, expand and constrain: Three principles for weakly-supervised image segmentation. In: *ECCV*, pp 695–711
- Krähenbühl P, Koltun V (2011) Efficient inference in fully connected crfs with gaussian edge potentials. In: *NeurIPS*, pp 109–117
- Ledig C, Theis L, Huszar F, Caballero J, Cunningham A, Acosta A, Aitken AP, Tejani A, Totz J, Wang Z, Shi W (2017) Photo-realistic single image super-resolution using a generative adversarial network. In: *CVPR*, pp 105–114
- Lee DD, Seung HS (1999) Learning the parts of objects by non-negative matrix factorization. *Nature* 401(6755):788–791
- Lee H, Huang J, Singh M, Yang M (2017) Unsupervised representation learning by sorting sequences. In: *ICCV*, pp 667–676
- Lee H, Lee K, Lee K, Lee H, Shin J (2021) Improving transferability of representations via augmentation-aware self-supervision. In: *NeurIPS*
- Lee J, Kim E, Lee S, Lee J, Yoon S (2019) FickleNet: Weakly and semi-supervised semantic image segmentation using stochastic inference. In: *CVPR*, pp 5267–5276
- Li K, Wu Z, Peng K, Ernst J, Fu Y (2018) Tell me where to look: Guided attention inference network. In: *CVPR*, pp 9215–9223
- Li X, Zhong Z, Wu J, Yang Y, Lin Z, Liu H (2019) Expectation-maximization attention networks for semantic segmentation. In: *ICCV*, pp 9166–9175
- Lin D, Dai J, Jia J, He K, Sun J (2016) ScribbleSup: Scribble-supervised convolutional networks for semantic segmentation. In: *CVPR*, pp 3159–3167
- Lin T, Maire M, Belongie SJ, Hays J, Perona P, Ramanan D, Dollár P, Zitnick CL (2014) Microsoft COCO: common objects in context. In: *ECCV*, Springer, vol 8693, pp 740–755
- Liu G, Lin Z, Yan S, Sun J, Yu Y, Ma Y (2012) Robust recovery of subspace structures by low-rank representation. *IEEE TPAMI* 35(1):171–184
- Long J, Shelhamer E, Darrell T (2015) Fully convolutional networks for semantic segmentation. In: *CVPR*, pp 3431–3440
- Ma L, Wang C, Xiao B, Zhou W (2012) Sparse representation for face recognition based on discriminative low-rank dictionary learning. In: *CVPR, IEEE*, pp 2586–2593
- O Pinheiro PO, Almahairi A, Benmalek R, Golemo F, Courville AC (2020) Unsupervised learning of dense visual representations. In: Larochelle H, Ranzato M, Hadsell R, Balcan MF, Lin H (eds) *NeurIPS*, vol 33, pp 4489–4500
- Ouali Y, Hudelot C, Tami M (2020) Semi-supervised semantic segmentation with cross-consistency training. In: *CVPR*, pp 12671–12681
- Papandreou G, Chen L, Murphy KP, Yuille AL (2015) Weakly-and semi-supervised learning of a deep convolutional network for semantic image segmentation. In: *ICCV*, pp 1742–1750
- Paszke A, Gross S, et al FM (2019) Pytorch: An imperative style, high-performance deep learning library. In: *NeurIPS*, pp 8024–8035
- Pathak D, Krähenbühl P, Donahue J, Darrell T, Efros AA (2016) Context encoders: Feature learning by inpainting. In: *CVPR*, pp 2536–2544
- Pinheiro PHO, Collobert R (2015) From image-level to pixel-level labeling with convolutional networks. In: *CVPR*, pp 1713–1721
- Saleh F, Akbarian MSA, Salzmann M, Petersson L, Gould S, Alvarez JM (2016) Built-in foreground/background prior for weakly-supervised semantic segmentation. In: *ECCV*, vol 9912, pp 413–432
- Shimoda W, Yanai K (2019) Self-supervised difference detection for weakly-supervised semantic segmentation. In: *ICCV*, pp 5207–5216
- Sohn K, Berthelot D, Carlini N, Zhang Z, Zhang H, Raffel C, Cubuk ED, Kurakin A, Li C (2020) Fixmatch: Simplifying semi-supervised learning with consistency and confidence. In: Larochelle H, Ranzato M, Hadsell R, Balcan M, Lin H (eds) *NeurIPS*
- Souly N, Spampinato C, Shah M (2017) Semi supervised semantic segmentation using generative adversarial network. In: *ICCV*, pp 5689–5697

- Stretcu O, Leordeanu M (2015) Multiple frames matching for object discovery in video. In: Xie X, Jones MW, Tam GKL (eds) *BMVC*, pp 186.1–186.12
- Su H, Jampani V, Sun D, Gallo O, Learned-Miller E, Kautz J (2019) Pixel-adaptive convolutional neural networks. In: *CVPR*, pp 11166–11175
- Sun G, Wang W, Dai J, Gool LV (2020) Mining cross-image semantics for weakly supervised semantic segmentation. In: *ECCV*, pp 347–365
- Tai C, Xiao T, Zhang Y, Wang X, Weinan E (2016) Convolutional neural networks with low-rank regularization. In: *ICLR*
- Vaswani A, Shazeer N, Parmar N, Uszkoreit J, Jones L, Gomez AN, Kaiser L, Polosukhin I (2017) Attention is all you need. In: *NeurIPS*, pp 5998–6008
- Wang X, Liu S, Ma H, Yang M (2020a) Weakly-supervised semantic segmentation by iterative affinity learning. *IJCV* 128(6):1736–1749
- Wang X, Zhang R, Shen C, Kong T, Li L (2021) Dense contrastive learning for self-supervised visual pre-training. In: *CVPR*, pp 3024–3033
- Wang Y, Zhang J, Kan M, Shan S, Chen X (2020b) Self-supervised equivariant attention mechanism for weakly supervised semantic segmentation. In: *CVPR*, pp 12272–12281
- Wei Y, Feng J, Liang X, Cheng M, Zhao Y, Yan S (2017) Object region mining with adversarial erasing: A simple classification to semantic segmentation approach. In: *CVPR*, pp 6488–6496
- Wei Y, Xiao H, Shi H, Jie Z, Feng J, Huang TS (2018) Revisiting dilated convolution: A simple approach for weakly- and semi-supervised semantic segmentation. In: *CVPR*, pp 7268–7277
- Wei Y, Zheng S, Cheng M, Zhao H, Wang L, Ding E, Yang Y, Torralba A, Liu T, Sun G, Wang W, Gool LV, Bae W, Noh J, Seo J, Kim G, Zhao H, Lu M, Yao A, Guo Y, Chen Y, Zhang L, Tan C, Ruan T, Gu G, Wei S, Zhao Y, Dobko M, Viniavskiy O, Doboševych O, Wang Z, Chen Z, Gong C, Yan H, He J (2020) LID 2020: The learning from imperfect data challenge results. *CoRR* abs/2010.11724, [2010.11724](https://arxiv.org/abs/2010.11724)
- Wu Z, Shen C, Van Den Hengel A (2019) Wider or deeper: Revisiting the ResNet model for visual recognition. *PR* 90:119–133
- Xie E, Ding J, Wang W, Zhan X, Xu H, Sun P, Li Z, Luo P (2021a) Detco: Unsupervised contrastive learning for object detection. In: *ICCV*, pp 8392–8401
- Xie Z, Lin Y, Zhang Z, Cao Y, Lin S, Hu H (2021b) Propagate yourself: Exploring pixel-level consistency for unsupervised visual representation learning. In: *CVPR*, pp 16684–16693
- Zheng S, Jayasumana S, Romera-Paredes B, et al (2015) Conditional random fields as recurrent neural networks. In: *ICCV*, pp 1529–1537
- Zhou B, Khosla A, Lapedriza A, Oliva A, Torralba A (2016) Learning deep features for discriminative localization. In: *CVPR*, pp 2921–2929
- Zhou B, Zhao H, Puig X, Xiao T, Fidler S, Barriuso A, Torralba A (2019) Semantic understanding of scenes through the ADE20K dataset. *IJCV* 127(3):302–321
- Zoph B, Ghiasi G, Lin T, Cui Y, Liu H, Cubuk ED, Le Q (2020) Rethinking pre-training and self-training. In: Larochelle H, Ranzato M, Hadsell R, Balcan M, Lin H (eds) *NeurIPS*
- Zou Y, Zhang Z, Zhang H, Li C, Bian X, Huang J, Pfister T (2021) Pseudoseg: Designing pseudo labels for semantic segmentation. *ICLR*